Computational Analysis of Shell Components in a Single Shell-and-Tube Heat Exchanger

Leon Chee Wai[1], Ong Wei Ming[1], Ishkrizat Taib[1,*], Leong Kit Sern[1]

[1] Department of Mechanical Engineering, Faculty of Mechanical and Manufacturing Engineering, Universiti Tun Hussein Onn Malaysia, 86400, Parit Raja, Johor, Malaysia

ARTICLE INFO	ABSTRACT
	This study investigates the optimisation parameters of a single-segment baffle, one-pass shell-and-tube counterflow heat exchanger, which is commonly used in industry. The objective was to minimise the pressure drop while optimising the heat transfer efficiency by using suitable tube arrangements, baffle cuts, and baffle inclination angles. The overall heat transfer coefficient, and total heat transfer rate, and were calculated using the logarithmic mean temperature difference (LMTD) method. ANSYS FLUENT v19.2 and SOLIDWORKS 2018 were used to simulate incompressible liquid water model under steady-state conditions. The tested parameters included tube arrangements at 20°, 45°, 60°, and 90°; baffle cuts at 25% and 36%; and baffle inclination angles at 0°, 20°, and 30°. The results indicated that the combination of a 90° tube arrangement, a 25% baffle cut, and a 20° baffle inclination provided optimal performance based on the experimental setup. The results of this research provide insights into enhancing the efficiency of shell-and-tube heat exchangers, thereby addressing issues related to the complexity of the shell-side geometry.

1. Introduction

Heat exchangers have been crucial mechanical components in the industry for many years [1-3]. Various types of heat exchangers exist, including double-pipe, spiral, plate-and-frame, plate-fin, and compact heat exchangers [4]. However, shell-and-tube heat exchangers are still widely used in industry. The design and optimisation of shell-and-tube heat exchangers primarily focuses on maximizing the heat transfer capacity while minimising the pressure drop [5]. This balance is crucial because an increased pressure drop leads to higher pumping power requirements, which contradicts the cost reduction goals.

Optimising the shell of heat exchangers presents unique challenges because of their structural complexity [6]. One key element within the shell is the baffle, which can be of various types: segmental, rod, disc, doughnut, and helical [7-9]. Baffles serve multiple purposes, such as directing fluid flow within the shell, maintaining effective circulation, optimising the heat transfer rate,

---

* Corresponding author.
E-mail address: iszat@uthm.edu.my

minimising heat exchanger vibration, and providing structural integrity [10]. Despite these innovations, single-segment baffles remain the most common in the industry.

Researchers have made significant contributions to improving shell components: Pressure drop investigations [5], development of novel software for heat transfer and pressure drop studies [4], exploration of angled baffles for increased heat transfer [11], and optimization of baffle spacing using thermoeconomic analysis [12]. Although most studies were experimental, some researchers opted for Computational Fluid Dynamics (CFD) approaches [6].

Modelling industrial heat exchangers using CFD is challenging because of high computational demands. However, an appropriate simplification can yield accurate predictions at reasonable computational costs. Three-dimensional modelling of the shell component fluid is crucial for identifying the localised recirculation that worsens the pressure drop [13].

This study aims to optimise the shell compartment of single-segmental baffle shell-and-tube heat exchangers with minimal structural and material addition. The objectives are to determine a suitable tube arrangement, baffle cut (Bc %), and baffle inclination angle to minimise the pressure drop while optimising the heat transfer rate. The overall heat transfer coefficient (U) and total heat transfer rate (Q̇) for the heat exchanger models were calculated using the LMTD method.

Furthermore, previous studies have often focused on individual aspects of optimisation, a few have investigated the combination of sequential geometric changes in the shell component. This study aimed to determine the optimal combination of tube arrangement, baffle cutting, and baffle inclination [14]. Halle *et al.,* [5] described four types of arrangement as 30°, 45°, 60°, and 90°. However, the 45° and 60° tube arrangements decreased the pressure drop by 10%. According to Zhang *et al.,* [15]The decrease in the baffle cut from 36% to 25% slightly improved the heat exchanger performance. Sadeghianjahromi *et al.,* [16] reported that increasing the baffle inclination can improve the heat transfer coefficient by 18.89%.

The present study employs the LMTD and ε-NTU methods to calculate heat exchanger performance parameters. Any modifications to the optimised heat exchanger will be evaluated based on the estimated cost reductions in pumping and heating power compared to increased material costs [17].

2. Methodology
2.1 Simulation Software

This research project relied entirely on simulation software, with ANSYS Workbench 19.2 being the primary tool. The ANSYS Workbench suite includes design modeller, mechanical, fluent, and CFD post, which were instrumental in conducting this study. Additionally, SolidWorks, a third-party CAD software, was used for heat exchanger modeling due to its familiarity and intuitive interface. This study adopted a history-based modeling approach. Table 1 lists the software used in this study.

Table 1
Software involves

Process	Software
Geometry creation	SolidWorks 2018
Geometry operation	ANSYS v19.2 design modeler
Meshing	ANSYS v19.2 mechanical
Solver	ANSYS v19.2 fluent
Post processing	ANSYS v19.2 CFD post
Report writing	MS Excel and MS Word 2019

2.2 Heat Exchanger Geometry

This study benchmarked Ozden's results as a reference to reproduce the exact geometrical model mentioned in Ozden's paper [6]. Table 2 summarises the dimensions of the geometrical model. In total, 24 models were created for simulation. Figure 1 illustrates the first geometry modelled based on Table 2 dimensions using SolidWorks and the imported IGES file format in the ANSYS design modeller.

Table 2
Heat exchanger dimensions

Heat exchanger shell's dimension	Values
Shell size, D_s	90 mm
Tube outer diameter, d_o	20 mm
Tube bundle geometry and pitch	Triangular 30°,30 mm
Number of tubes, N_t	7
Heat exchanger length, L	600 mm
Baffle cut, B_c	36%
Central baffle spacing, B	86 mm
Number of baffles, N_b	6

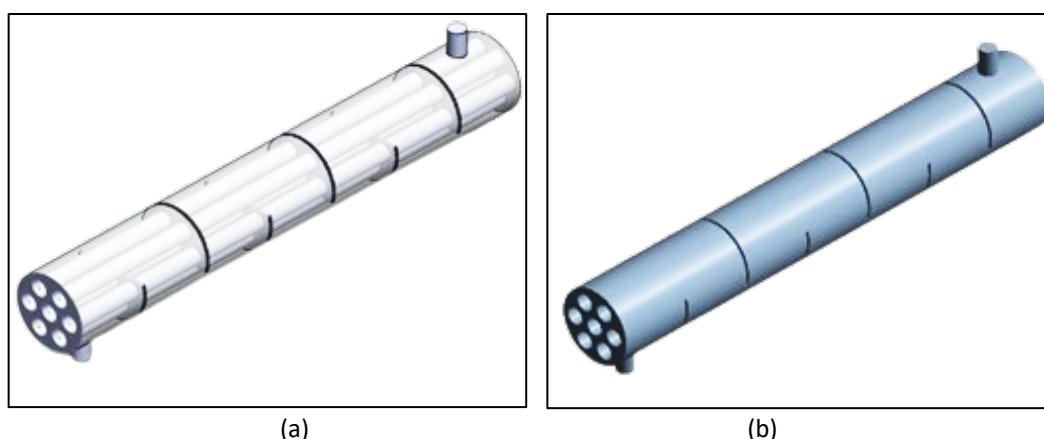| (a) | (b) |

Fig. 1. Heat exchanger shell geometry (a) SolidWorks creation (b) ANSYS design modeler imported

2.2.1 Model cleaning and repair

Quality checks were performed on all specimens to remove any edges, sharp angles, slivers, and holes. Table 3 lists entries for allowable geometric entities using relevant repair tools. The clean-up process eliminated unnecessary slivers, holes, and sharp angles although two small edges were detected on the inlet, as shown in Figure 2.

Table 3
Geometry cleaning check

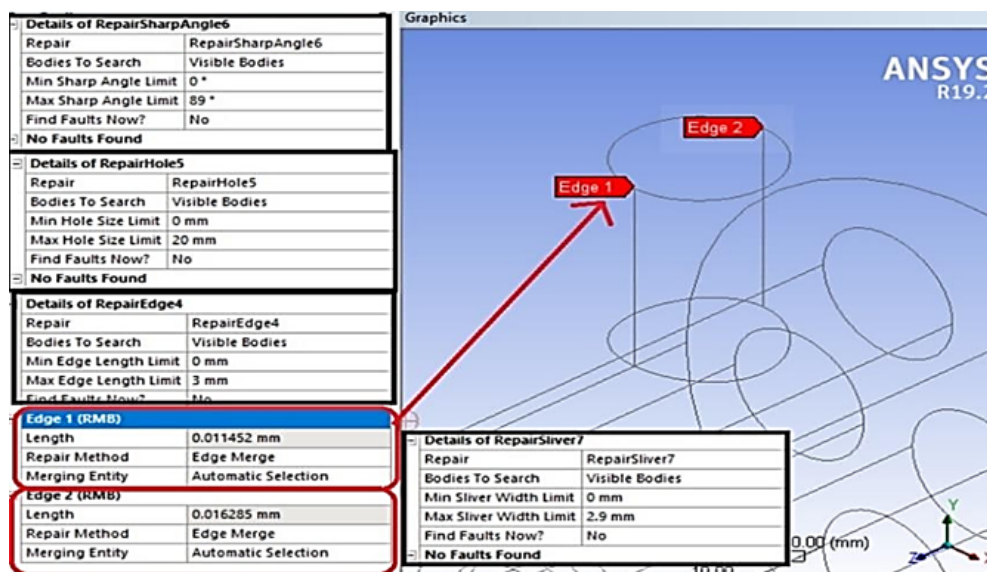| Geometry repair and clean up tool	Smallest allowable entity
Small edges	Baffle thickness, 3 mm
Slivers	Baffle thickness, 3 mm
Holes	Tube diameter, 20 mm
Sharp angles	Maximum allowable angle, 90°

Fig. 2. Geometric cleaning of heat exchanger geometry

2.2.2 Relevant 3D operations

Several operations were conducted to prepare the mesh, and various techniques were tested before running the simulation, including hexahedral meshing and inflation layers. To obtain the total hexahedral specimen, slicing operations were required to create sweepable bodies, as shown in Figure 3.
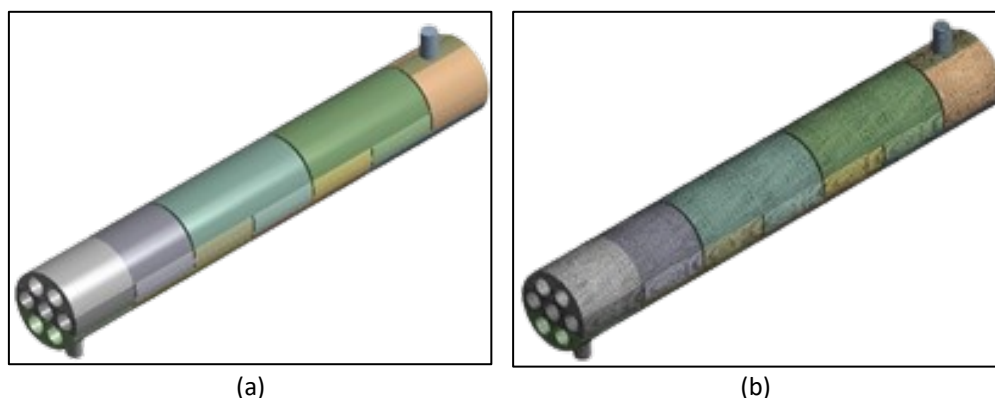

| (a) | (b) |

Fig. 3. Heat exchanger (a) Sliced geometry (b) Hexahedral dominant mesh geometry

Due to the instability of the pure hexahedral mesh, the project switched to pure tetrahedral meshing for the remaining models. 3D operations included creating bodies in targeted regions to increase the mesh density using the body-of-influence setting to capture salient turbulent secondary flow features with precision, as illustrated in Figure 4.
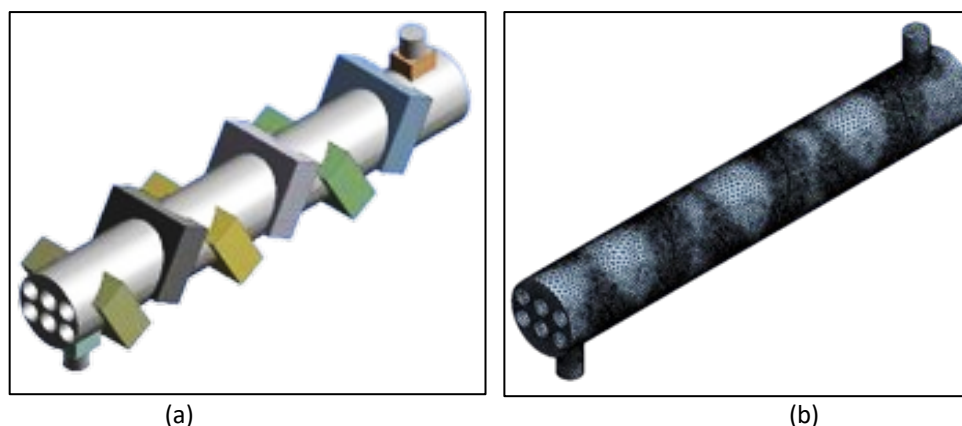
Fig. 4. Geometry of influence creation: (a) Heat exchanger (b) Tetrahedral mesh distribution

2.3 Geometry Discretization
2.3.1 Meshing method

Several meshing approaches are available, including sweeping, hex-dominant, tetrahedral, multizone, and automatic methods. In the preliminary stage of meshing the default mesh models (DM), an automatic method was employed. Due to the non-sweepable nature of the model body, the resulting DM mesh was purely tetrahedral. For the subsequent refined mesh models (RM), the tetrahedral method with a patch conforming algorithm was used to ensure that all faces and boundaries were captured and conformed. This approach was selected because the patch conforming algorithm uses a bottom-up approach: meshing edges first, then faces, and finally the volume of the model. Figure 5 presents the settings for the RM models.
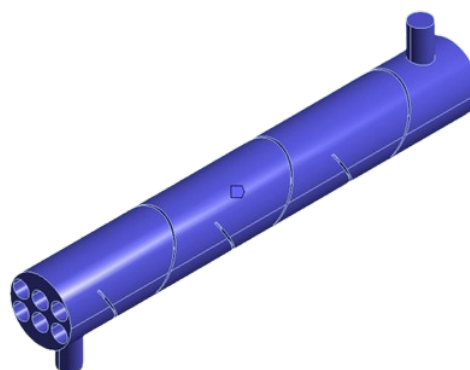

Fig. 5. Refined mesh models

2.3.2 Global mesh settings

For the global mesh settings, the physics preference was set to CFD with the solver preference of FLUENT. The element size was set to 20 mm, which is sufficiently small. Given the circular nature of the shell geometry with numerous curvatures, the curvature capture option was enabled with the curvature normal angle set to 18°. However, the proximity capture option was disabled because the proximity features near the baffle regions were refined using local mesh settings, specifically, the body of influence, as shown in Figure 5. The inflation option was turned off for further evaluation in the local mesh settings. The growth rate was left at the default value of 1.2 because reducing it refines the entire model, which significantly increases computational cost. For mesh defeaturing, the default

setting of 0.1 mm was used to capture all features greater than 0.1 mm. Any mesh size reduction would induce unnecessary global refinement. Figure 6 shows a sample of the global mesh settings used in this study.

Fig. 6. Global mesh setting

2.3.3 Local mesh settings

The local mesh settings in this study involved body sizing and inflation. Although inflation was tested during the trial runs, inflation was ultimately not used because of inaccuracies during the verification process. Wall regions typically have boundary-layer flow features due to the presence of inviscid flow assumptions. Initially, 10 boundary inflation layers (as recommended by ANSYS) were introduced on the shell-geometry walls (see Figure 7).

However, because the extracted data did not focus on near-wall regions, inflation layers were deemed unnecessary. In addition, because inflation layers induced inaccuracies, they were excluded from the actual run, which reduced the number of elements and improved the model mesh quality. Most importantly, the introduction of inflation layers was found to be harmful to mesh quality [17].

Fig. 7. Initial inflation layers

2.4 Boundary Conditions

The boundary condition parameters are listed in Table 4.

Table 4
Boundary condition parameter

Setting	Type	Specifications
Boundary conditions		
Shell inlet	Mass flow rate	Turbulence intensity: 5%
		Temperature: 300 K
Shell outlet	Pressure outlet	Gauge pressure 0 Pa
Tube walls	Wall	Temperature: 450 K
Pressure-velocity coupling		
Method	SIMPLE	Used due to its robustness and memory efficiency for relatively simple steady-state flows
Initialization		
Method	Standard initialization	Set up initial conditions based on boundary settings

3. Results

The simulation results were presented using quantitative and qualitative approaches. The quantitative approach was crucial for demonstrating the heat exchanger performance by comparing the overall heat transfer coefficient U and the total heat transfer rate, $\dot{Q}$. The qualitative approach involves displaying contours and velocity streamlines to illustrate the flow phenomena in the heat exchanger shell geometry.
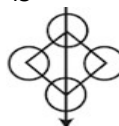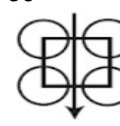
3.1 Quantitative Comparison

The quantitative comparison was divided into three stages. The key results are summarized in Table 5. To facilitate data understanding, Table 6 was prepared using the defender-challenger mode of comparison. Based on the results, the 90° tube arrangement recorded the lowest pressure increment among the challengers (26.27% relative to 45° and 60°). Although not the best for $\dot{Q}$ and U increments, it ranked second after 60°. The 90° tube arrangement was chosen due to its significantly lower pressure drop increment compared to the 60° arrangement (30.39% lower), while only falling short by 2.03% and 2.32% for $\dot{Q}$ and U, respectively.

Table 5
Stage 1 tube arrangement

Tube Arrangement	Raw data				Processed data			
	$T_{in,\,avg}$ (K)	$T_{out,\,avg}$ (K)	$P_{in,\,avg}$ (Pa)	$P_{out,\,avg}$ (Pa)	ΔP (Pa)	LMTD (K)	$\dot{Q}$ (W)	U (W/(m²K))
30°	300	331.68	6180.6	0	6180.6	133.53	132494	3851.7
45°	300	332.19	8385.5	0	8385.5	133.26	134183	3913.4
60°	300	336.08	9682.3	0	9682.3	131.13	150896	4466.1
90°	300	335.46	7804.5	0	7804.5	131.48	148203	4376.7

Table 6

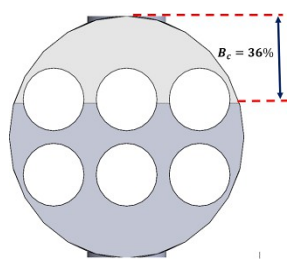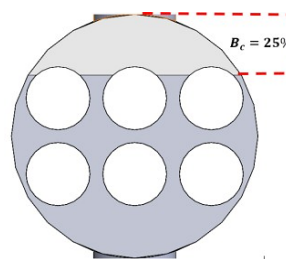Comparison and selection of optimized tube arrangement

	Defender	Challengers		
Parameters	30°	45°	60°	90°
Total heat transfer rate, $\dot{Q}$ (W)	132494	134183	150896	148203
Overall heat transfer coefficient, U ($W/m^2 . K$)	3851.66	3913.42	4466.09	4376.68
Pressure drop, ΔP	6180.64	8385.48	9682.33	7804.54
ΔP Increment (%)		35.67	56.66	26.27
$\dot{Q}$ Increment (%)		1.27	13.89	11.86
U Increment (%)		1.60	15.95	13.63

In stage 2, the investigation focused on comparing the changes in the baffle cut alterations from 36% and 25%. Tables 7 and 8 present the key results and percentage comparisons, respectively. Lowering the baffle cut to 25% decreased the pressure drop by 1.72%, with a negligible $\dot{Q}$ decrement of 0.09% and U increase of 0.39%. This finding aligns with [11] conclusion that a 25% baffle cut is superior to a 36% cut. The prediction was more accurate, describing the slight improvement observed with the 25% baffle cut.

Table7

Optimization stage 2 baffle cut results

Baffle Cut	Raw data				Processed data			
	$T_{in,avg}$ (K)	$T_{out,avg}$ (K)	$P_{in,avg}$ (Pa)	$P_{out,avg}$ (Pa)	ΔP (Pa)	LMTD (K)	$\dot{Q}$ (W)	U (W/(m²K))
36%	300	335.46	7804.5	0	7804.5	131.48	148203	4376.7
25%	300	335.41	7670.7	0	7670.7	131.50	148075	4393.7

Table 8

Comparison and selection of optimized baffle cut

	Defender	Challenger
Parameters	B_C = 36%	B_C = 25%
	(Using TA = 90°, θ_B = 0°)	(Using TA = 90°, θ_B = 0°)
Total heat transfer rate, $\dot{Q}$ (W)	148203	148075
Overall heat transfer coefficient, U ($W/m^2 . K$)	4376.68	4393.7
Pressure drop, ΔP	7804.54	7670.66
ΔP Increment (%)		-1.72
$\dot{Q}$ Increment (%)		-0.09
U Increment (%)		0.39

In Stage 3, the baffle inclination angles were examined to explore further optimisation opportunities. Table 9 lists the key results for the 20° and 30° inclination angles, whereas Table 10 presents a defender-challenger comparison. Increasing the baffle inclination angle helped reduce the pressure drop but at the cost of Q̇ and U decrements. For the 20° angle, the pressure drop decreased by 12.96%, outweighing the Q̇ and U decrements of 8.35% and 8.39%, respectively. This trend was similar to that reported by [11], who observed a 6% pressure drop when the angle was increased from 0° to 20°.

Table 9
Optimization stage 3 results of the baffle inclination angle

Baffle inclination angle	Raw data				Processed data			
	$T_{in,avg}$ (K)	$T_{out,avg}$ (K)	$P_{in,avg}$ (Pa)	$P_{out,avg}$ (Pa)	ΔP (Pa)	LMTD (K)	$\dot{Q}$ (W)	U ($W/(m^2K)$)
0°	300	335.41	7670.7	0	7670.7	131.50	148075	4393.7
20°	300	332.90	6762.1	0	6676.6	132.92	137201	4026.8
30°	300	333.12	7308.9	0	7308.9	132.75	138513	4070.4

Table 10
Comparison and selection of optimized baffle inclination angle

	Defender	Challengers	
Parameters	0° (Using TA = 90°, B_C = 25%)	20° (Using TA = 90°, B_C = 25%)	30° (Using TA = 90°, B_C = 25%)
Total heat transfer rate, $\dot{Q}$ (W)	148075	137201	138513
Overall heat transfer coefficient, U ($W/m^2.K$)	4393.7	4026.81	4070.39
Pressure drop, ΔP	7670.66	6676.64	7308.89
ΔP Increment (%)		-12.96	-4.72
$\dot{Q}$ Increment (%)		-8.35	-6.46
U Increment (%)		-8.39	-7.36

Subsequently, use angles greater than 20° because of possible compromise of structural integrity. The 30° angle showed a dramatic pressure reduction of 4.72% at the cost of decreasing Q̇ and U by 6.46% and 7.36%, respectively, indicating that angles beyond 20° were counterproductive [18]. Based on a quantitative comparison across the three optimisation stages, the CFD simulation data conclusively showed that a tube arrangement of 90° with a 25% baffle cut and a 20° baffle inclination angle was the optimised shell geometry for this project's heat exchanger model.
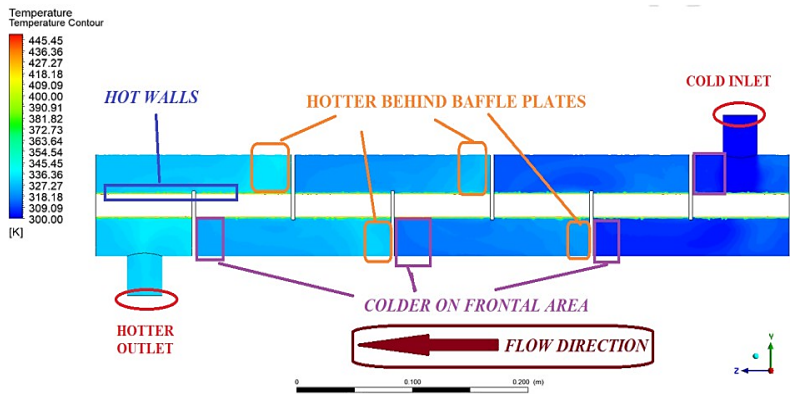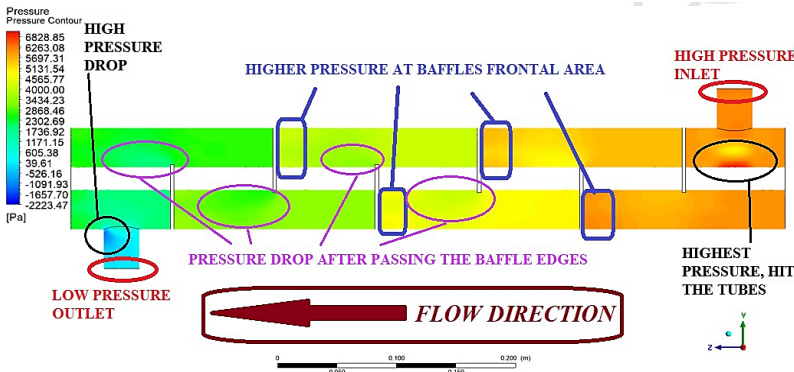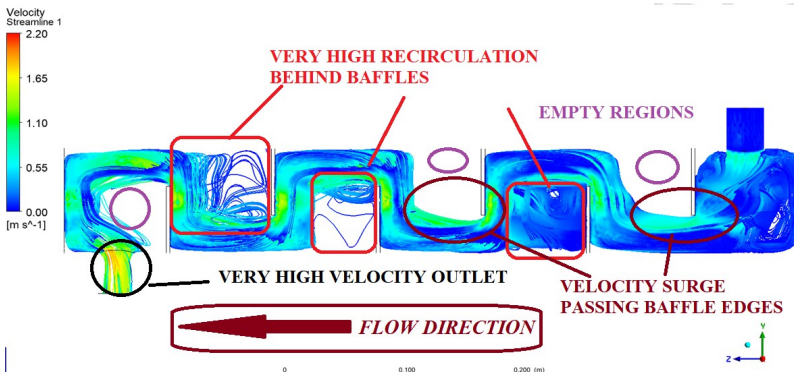
3.2 Qualitative Comparison

The quantitative comparison successfully achieved the objectives of determining the optimised shell geometry with a suitable tube arrangement, baffle cut, and baffle inclination angle. Table 11 displays the flow contours and velocity streamlines of the shell geometry for a 30° tube arrangement, 36% baffle cut, and 0° baffle inclination.

The observations listed in Table 11 indicate that the inlet temperature contour was lower than that of the outlet nozzle, indicating heat conduction and convection from the tube walls to the shell fluid. Notably, the fluid temperature on baffle surfaces facing opposite the flow direction was lower than that in regions parallel to the fluid flow direction [18]. This phenomenon was attributed to the high fluid velocity impacting the baffle surface opposite the flow direction, resulting in forced convection that accelerated the temperature drop [19].

Conversely, regions facing parallel to the flow exhibited higher temperatures because of the slower flow velocity, which dampened heat dissipation. The pressure contour exhibited a dramatic drop from the inlet to the outlet and an increased pressure distribution near the wall regions, including the tube and shell walls. This pressure distribution trend was correlated with the velocity streamline distribution, where the no-slip conditions at the walls reduced the flow velocity in the near-wall regions. According to Bernoulli's principle, the pressure increases as the flow velocity decreases. These observations were typical across all specimens, with the three visual aids closely linked to each other.

Table 11
Qualitative comparison of visual aids

Item	Visual aids
	Shell geometry with a 30° tube arrangement, a 36% baffle cut, and a 0° baffle inclination angle
Temperature contour	
Pressure contour	
Velocity streamline	

4. Conclusions

In this study, the optimal parameters for a shell-and-tube heat exchanger were determined. The results indicate that a 90° tube arrangement, 25% baffle cut, and a 20° baffle inclination significantly enhanced the performance by reducing the pressure drop and optimising heat transfer. The CFD simulations confirmed the accuracy of these parameters, demonstrating a pressure drop reduction of 12.96% at 20° inclination. Furthermore, this study achieved its educational objectives by equipping students with fundamental CFD skills to solve industrial flow problems. Additional experiments are recommended for different heat exchanger designs and operating conditions.

Acknowledgement

References

[1] Cengel, Yunus A., and Afshin J. Ghajar. "Introduction and basic concepts." In *Heat and Mass Transfer Fundamental and Applications*, pp. 7-10. New York, NY, USA: McGraw-Hill Education, 2015.

[2] Mousa, Mohamed H., Nenad Miljkovic, and Kashif Nawaz. "Review of heat transfer enhancement techniques for single phase flows." *Renewable and Sustainable Energy Reviews* 137 (2021): 110566. https://doi.org/10.1016/j.rser.2020.110566

[3] Javadi, Hossein, Seyed Soheil Mousavi Ajarostaghi, Marc A. Rosen, and Mohsen Pourfallah. "Performance of ground heat exchangers: A comprehensive review of recent advances." *Energy* 178 (2019): 207-233. https://doi.org/10.1016/j.energy.2019.04.094

[4] Karno, A., and S. Ajib. "Effect of tube pitch on heat transfer in shell-and-tube heat exchangers—new simulation software." *Heat and mass transfer* 42 (2006): 263-270. https://doi.org/10.1007/s00231-005-0002-9

[5] Halle, H., J. M. Chenoweth, and M. W. Wambsganss. "Shellside waterflow pressure drop distribution measurements in an industrial-sized test heat exchanger." *Jounal of Heat and Mass Transfer* 110, no. 1 (1988): 60-67. https://doi.org/10.1115/1.3250474

[6] Ozden, Ender, and Ilker Tari. "Shell side CFD analysis of a small shell-and-tube heat exchanger." *Energy conversion and management* 51, no. 5 (2010): 1004-1014. https://doi.org/10.1016/j.enconman.2009.12.003

[7] Mohammadi, Mohammad Hadi, Hamid Reza Abbasi, Adel Yavarinasab, and Hossein Pourrahmani. "Thermal optimization of shell and tube heat exchanger using porous baffles." *Applied Thermal Engineering* 170 (2020): 115005. https://doi.org/10.1016/j.applthermaleng.2020.115005

[8] Marzouk, S. A., M. M. Abou Al-Sood, Magda K. El-Fakharany, and Emad MS El-Said. "A comparative numerical study of shell and multi-tube heat exchanger performance with different baffles configurations." *International Journal of Thermal Sciences* 179 (2022): 107655. https://doi.org/10.1016/j.ijthermalsci.2022.107655

[9] Kaleru, Aparna, Sriram Venkatesh, and Narasimha Kumar. "Numerical and experimental study of a shell and tube heat exchanger for different baffles." *Heat Transfer* 52, no. 3 (2023): 2186-2206. https://doi.org/10.1002/htj.22780

[10] Mohanty, Shuvam, and Rajesh Arora. "CFD analysis of a shell and tube heat exchanger with single segmental baffles." *International Journal of Automotive and Mechanical Engineering* 17, no. 2 (2020): 7890-7901. https://doi.org/10.15282/ijame.17.2.2020.08.0589

[11] Irshad, Mohammed, Mohammed Kaushar, and G. Rajmohan. "Design and CFD analysis of shell and tube heat exchanger." *International Journal of Engineering Science and Computing* 7, no. 4 (2017): 6453-6457.

[12] Eryener, Dogan. "Thermoeconomic optimization of baffle spacing for shell and tube heat exchangers." *Energy Conversion and Management* 47, no. 11-12 (2006): 1478-1489. https://doi.org/10.1016/j.enconman.2005.08.001

[13] Singh, Gurbir, and Hemant Kumar. "Computational fluid dynamics analysis of shell and tube heat exchanger." *Journal of Civil Engineering and Environmental Technology* 1, no. 3 (2014): 66-70.

[14] Arani, Ali Akbar Abbasian, and Reza Moradi. "Shell and tube heat exchanger optimization using new baffle and tube configuration." *Applied Thermal Engineering* 157 (2019): 113736. https://doi.org/10.1016/j.applthermaleng.2019.113736

[15] Zhang, Ji, Xiaowei Zhu, Maria E. Mondejar, and Fredrik Haglind. "A review of heat transfer enhancement techniques in plate heat exchangers." *Renewable and Sustainable Energy Reviews* 101 (2019): 305-328. https://doi.org/10.1016/j.rser.2018.11.017

[16]   Sadeghianjahromi, Ali, and Chi-Chuan Wang. "Heat transfer enhancement in fin-and-tube heat exchangers–A review on different mechanisms." *Renewable and Sustainable Energy Reviews* 137 (2021): 110470. https://doi.org/10.1016/j.rser.2020.110470

[17]   Pfaff, Tobias, Meire Fortunato, Alvaro Sanchez-Gonzalez, and Peter W. Battaglia. "Learning mesh-based simulation with graph networks." *arXiv preprint arXiv:2010.03409* (2020). https://doi.org/10.48550/arXiv.2010.03409

[18]   Menni, Younes, A. Chamkha, Chafika Zidani, and Boumédiène Benyoucef. "Baffle orientation and geometry effects on turbulent heat transfer of a constant property incompressible fluid flow inside a rectangular channel." *International Journal of Numerical Methods for Heat & Fluid Flow* 30, no. 6 (2020): 3027-3052. https://doi.org/10.1108/HFF-12-2018-0718

[19]   Menni, Younes, Ahmed Azzi, Ali Chamkha, and Souad Harmand. "Analysis of fluid dynamics and heat transfer in a rectangular duct with staggered baffles." *Journal of Applied and Computational Mechanics* 5, no. 2 (2019): 231-248. https://doi.org/10.22055/jacm.2018.26023.1305